NPA/Int. 63-11
Meyrin, 6th May 1963

NEUTRINO FLUX CALCULATIONS

Summary :

A description is given of the method used for calculating the neutrino flux at the detectors, taking into account the focusing provided by the neutrino horn. Results of the computations for various experimental conditions are presented.

1. Method of calculating neutrino flux

1.1 General procedure

Secondaries coming from the target inside the horn are traced through the horn. This is done for particles of different momentum, from different parts of the target, and with different emission angles. The absorption probability in target and horn material is computed for each particle, as well as its angle with the axis after the horn. These figures are then combined with the (given) production spectrum and with the probability of production for each part of the target. The result are the angular spectra of secondaries after the horn, for different momentum values.

In order to compute the neutrino flux at the detector, the decay path is now divided into several sections, and the probability of decay for each section is determined. This is then combined with the angular spectrum mentioned above. For different angles the probability that the neutrino hits the detector is computed. This is done for different regions of the detector cross section (at different distances from the axis). The neutrino momentum is also computed at this stage, since it is a function of decay angle. The whole procedure is repeated for each section of the decay path, and for different momentum values. Finally the neutrino spectrum at the detector, averaged over a certain cross section, is obtained.

The limited width of the decay path is taken into account.

1.2 Approximations used

a) Production spectrum

For the results presented in this report, the pion spectrum according to the formulae proposed by G. von Dardel (1) was used. These formulae are :

$$\frac{\delta^2 N}{\delta p \delta \omega} = 0.2\, P_o\, e^{-p(0.25 + 25\vartheta^2)} \qquad \text{for } p < 3 \text{ GeV/c}$$

$$\frac{\delta^2 N}{\delta p \delta \omega} = \frac{k}{\pi} \cdot \frac{p^2 (P_o - p)}{p_o T^2 (P_o - 2T)}\, e^{-p\left(\frac{1}{T} + \frac{\vartheta^2}{p_o}\right)} \qquad \text{for } p \geq 3 \text{ GeV/c}$$

with P_o = primary momentum

$p_o = 0.0445$ GeV/c

$T = 0.9 + 0.034\, P_o$

$k = 0.13 + 0.013\, P_o$

(all momenta in GeV/c, angles in rad)

This spectrum is in good agreement with measurements at CERN (2) and Brookhaven (3) on targets of light material (Be, Al). In the horn a heavy material (Ir) target will have to be used; the production spectrum might therefore be somewhat different.

The spectrum refers to one polarity only. It is supposed to be the same for positive and negative pions.

The K - spectra were computed from the π - spectra, using the K/π ratios as shown in fig. 1. These are mainly based upon data from ref. (3). Some discrepancy exists between different measurements of this ratio, and they should probably not be trusted too much.

For the final evaluation of the neutrino experiments, the latest production spectra will have to be used. The results given in this report should therefore be considered as preliminary.

b) Absorption in target

The target will be a cylinder with a diameter of 4 mm and a length of 200 mm. This corresponds to about 2.4 interaction lengths. It was established that this is an optimum value.

The secondaries leave the target mostly through the cylindrical surface, but partly through the end. For each particle considered in the calculation, the average path in the target is determined. The chance that it will interact, and therefore be lost, is taken into account.

Some low energy particles originating in the first part of the target, will be deflected so strongly by the horn, that they will cross the target a second time. The extra absorption caused in this way is also taken into account.

c) Multiple interactions

It is possible that an appreciable fraction of the protons that have interacted will still have sufficient energy left to contribute to the secondary flux by interacting again. This extra contribution was not taken into account.

d) Tertiary particles

These particles, produced when secondaries interact in the target or horn material, were neglected.

e) Scattering of protons in target

It is thought that most of the protons will hit the target inside a diameter of 3 mm. The target is 4 mm wide (but its width might be increased to a maximum of 5.5 mm if it were necessary). The angular spread of the proton beam will cause a divergence inside the target of a few tenth of a mm only. By multiple scattering and diffraction scattering the beam might be blown up somewhat more, and before the end of the target a small percentage of the protons might leave it sideways. However, few of the protons will ever reach the end of the

target without interacting, since the interaction length (for absorption only) is about 8.3 cm in iridium. Therefore, this effect has been neglected. Of course, much depends upon the spot size that will actually be achieved.

f) Off-centre particles

In the calculation it is assumed that all secondaries are produced on the axis of the target. Particles produced off-centre will on the average traverse less target material before leaving the target (see fig. 2). The effect is small, however, and therefore neglected.

The trajectories through the horn will also be somewhat different for particles that are not coplanar with the axis. This effect was checked and found to be small. It was neglected.

g) Dependence on location in target where particle is produced. The target is 200 mm long. For the flux calculations it is divided into 5 parts, each of which is treated separately, as if the secondaries originated in its centre. An average is then computed, applying proper weighting factors to the 5 parts of the target.

h) Thickness of inner conductor

The current in the inner conductor of the horn will flow mainly in a layer with a thickness of about 1.5 mm (skin effect). In the calculation it is supposed that the layer is infinitely thin and situated in the "centre of gravity" of the real current distribution.

The probability of absorption of the secondaries, as they cross the inner conductor, is computed as if the mass of the conductor were concentrated in this thin layer. This is not quite correct, since the actual trajectories are bent inside the conductor, and will therefore traverse more material when entering from the inside, and less when entering from the outside.

i) Absorption in flanges and bolts connecting the two parts of the inner conductor together, is neglected.

j) Production angles above 19° are neglected.

k) The cross section of the decay tunnel is supposed to be circular. This will cause a relatively small error, only at low neutrino momentum, since the shielding around the decay tunnel does not reduce the flux much.

l) Ejection efficiency

It is supposed that 90 o/o of the protons circulating in the PS will hit the target. All fluxes are given per circulating proton.

m) Scattering

Multiple scattering of secondaries in the material of the horn is neglected. On the average, the particles will traverse about one radiation length in aluminium before leaving. This will cause a r.m.s. scattering angle of about 0.02/p, if p is expressed in GeV/c. The probability of hitting the detector is inversely proportional with $(1 + \delta^2 \vartheta^2)^2$, if ϑ is the decay angle. By substituting the scattering angle for ϑ , it can be seen that, independently of momentum, the probability is hardly influenced.

The probability of diffraction scattering is rather small. It was therefore neglected, even though somewhat larger angles are involved.

n) Decay of particles inside the horn is neglected. The decay path is supposed to begin 2 m downstream from the target.

o) Quantisation of angles and momenta

In the type of numerical computation used, it is obviously impossible to consider a continuum of emission angles and particle momenta. Therefore, discrete values are taken. This involves approximations. Also, the intermediate angular spectra and the final neutrino momentum spectra are stored in tables with finite intervals. These intervals are as follows :

For pion (or kaon) momentum : 0.5 GeV/c (from 0.5 up to 12 GeV/c)
For emission angles : 0.25^{o}
For angular distribution after horn : 0.125^{o}
For neutrino momentum : 0.2 GeV/c

The influence of these finite intervals will be greatest at the low energy end of the neutrino spectrum.

The precision of the final results is mainly limited by approximation (a) (production spectrum). However, even though the other approximations will give rise to smaller individual errors, their great number might still cause an additional uncertainty of 20 - 30 o/o.

2. Results of computations

2.1 General

The results given here differ from earlier ones (4) mainly because the design of the horn was improved several times. It is now made so as to give optimum focusing for 6 GeV/c particles. This is a compromise between the desirability of a strong contribution from high energy neutrinos on the one hand, and from the low energy ones on the other. It would be possible to improve the high-energy tail of the spectrum still more ; the total counting rate might, however, go down in this case, since most neutrinos are low-energy ones.

The present shape of the horn is shown in fig. 21.

All results shown refer to the flux in the bubble chamber. In the spark chamber about 25 o/o less is expected, because of its greater distance from the horn (see par. 2.7 for more details).

Tables of neutrino flux as a function of neutrino momentum and radial position in the detector are available on IBM cards, for various PS energies, horn currents, particle types, etc. These can be used for evaluation of the experimental results.

2.2 Focusing properties of horn

Fig. 3 shows how the angle of the secondary particles with the horn axis after the horn behaves as a function of particle momentum and angle at the target (emission angle). This plot is valid for only one of the 5 target parts mentioned above, and should therefore be considered as an illustration of the general behaviour of the horn rather than as a complete definition of its properties.

The complicated shape of the curves is due to the shape of the inner conductor (with discontinuities in slope ; see fig. 4) and to the fact that the particles may emerge either through one of the conical parts of the inner conductor, through the end plate, or even through the outer conductor. Moreover, at lower momenta a particle may enter and leave the field between inner and outer conductor two times. In fig. 4 these different"modes" are numbered and in fig. 5, which shows the same curves as fig. 3, the areas corresponding to each of these modes are indicated with the same numbers.

It will be seen that the best focusing action corresponds to regions IV and V. Most of the secondaries are emitted in these regions, except at lower momenta where in any case the requirements on the precision of focusing are less exacting.

Fig. 6 shows the same plot for the particles of the opposite sign, which are defocused. The discontinuities in the curves are caused by the discontinuities in the shape of the outer conductor.

Figs 7 - 11 show the expected intensity as a function of angle with the axis for the focused pions, fig. 12 for the defocused ones. These diagrams refer to operation with a horn current of 300 kA, and give the flux per circulating proton of 24.8 GeV/c. The irregularities in the curves are caused by the focusing characteristics of the horn and correspond with the discontinuities in fig. 3 and 6.

2.3 Neutrino flux as a function of horn current

Fig. 13 shows the neutrino flux in the bubble chamber for different currents in the horn. The maximum current is 300 kA.

The polarity of the current is such that positive particles are focused.

The flux shown here is the average value over a circular detector cross section with radius 0.4 m.

The flux is shown for neutrinos both from π^+ and from K^+ ; background from π^- and K^- is also indicated.

The curve marked " ideal focusing" refers to the flux that would be obtained if by some device all pions could be made parallel to the axis. For calculating this curve, the same target efficiency was assumed as with the actual set-up ; it was supposed that the hypothetical ideal focusing device would not absorb any particles. Again, the flux was averaged over the same detector area.

Fig. 14 shows the same for the case that negative particles are focused. The curves for neutrinos from pions are the same as those of fig. 13.

All curves are for a primary momentum of 24.8 GeV/c (i.e. 3 sec. repetition period).

By combining these curves with the cross section for elastic neutrino interactions (5) , it is found that the optimum current for these interactions is somewhere near 200 kA. The optimum is flat.

Of course, for studying intermediate boson production, full current should be used.

2.4 Dependence on machine energy

The neutrino flux was also calculated for a primary momentum of 28.4 GeV/c and 21.9 GeV/c. These values correspond to a 5 sec and 2 sec repetition period, respectively. In fig. 15 the results for three primary momenta are compared, for a horn current of 300 kA and positive particles.

The relative intensities depend, of course, on the assumptions about the production spectrum, i.e. on the "von Dardel" interpolation formulae mentioned in par. 1.2.

2.5 Dependence on detector radius

Fig. 16 shows how the neutrino flux in the bubble chamber changes as a function of the distance to the axis. The effect of this distance would be expected to be maximum for high-energy neutrinos, because their decay angles are smallest.

The cross-over of the curves at the far high-energy end of the spectrum is caused by the fact that in that region most of the pions and kaons are somewhat under-focused, as may be seen from fig. 3. Most of the secondaries of more than 7 GeV/c are still slightly divergent after the horn and cause therefore a relatively low neutrino flux in the exact centre of the detector.

At low momenta, the focusing is less precise, and decay angles are large ; therefore the detectors will be homogeneously illuminated with neutrinos.

In fig. 17 the average flux in a circular detector area is shown as a function of its radius.

All curves of fig. 16 and 17 refer to 300 kA, 24.8 GeV/c operation.

2.6 Dependence on length of decay tunnel

In fig. 18 is shown how the neutrino flux varies if the length of the decay tunnel (L_1 in fig. 19) would be varied, keeping the length of the shielding (L_2) constant. The horizontal scale gives the relative change with respect to the present situation ; in the same way the vertical scale gives the relative increase in intensity that would be obtained in this way. The different curves refer to different intervals of neutrino momentum.

It seems that the present length is near optimum, especially for K-neutrinos.

All curves were calculated for a primary momentum of 24.8 GeV/c, a horn current of 300 kA, and refer to the average flux over a detector section with radius 0.4 m.

2.7 Dependence on length of shielding

A diagram similar to the preceding one is given in fig. 20 for variations of the distance from the beginning of the shielding to the centre of the detector (L_2 in fig. 19). L_1 is supposed to be constant. The "normal" position of the detector, considered here (corresponding to zero on the horizontal scale), is the centre of the bubble chamber, as it is located at present.

All curves refer to the same conditions (primary momentum, etc) as those of par. 2.6.

For the centre of the first part of the spark chambers, L_2 is about 25 o/o greater than for the bubble chamber ; the relative neutrino intensity can therefore be found to be about 25 o/o less from fig. 20.

Obviously, large gains could be realised by decreasing L_2. However, it must be remembered that the distance from the downstream end of the screening to the centre of the detector is included in L_2. Therefore, even if somehow the thickness of the shield could be decreased to e.g. 5 m, with the present experimental set-up the gain would only be about a factor 3 for the bubble chamber, and a factor 2.5 for the spark chamber (for π - neutrinos of 1 - 2 GeV/c and K - neutrinos of 2 - 6 GeV/c).

S. van der Meer
K.M. Vahlbruch

/fv

Distribution : (open)
N.P.A. Scientific staff

PS/3805

References

1) NP/Internal Report 62-17
NP/Memo/378

2) "N 4" Experiment (A. Diddens, E. Lillethun, M. Manning, A. Taylor, Th. Walker A. Wetherell) ; unpublished

3) Baker et al., Phys. Rev. Letters 7, 101, 1961

4) CERN 61-7
NPA/Int. 62-7
NPA/Int. 62-11
Giesch et al., Nuclear Instr. and Methods 20, 58, 1963

5) Lee and Yang, Phys. Rev. Letters 4, 307, 1960

/fv

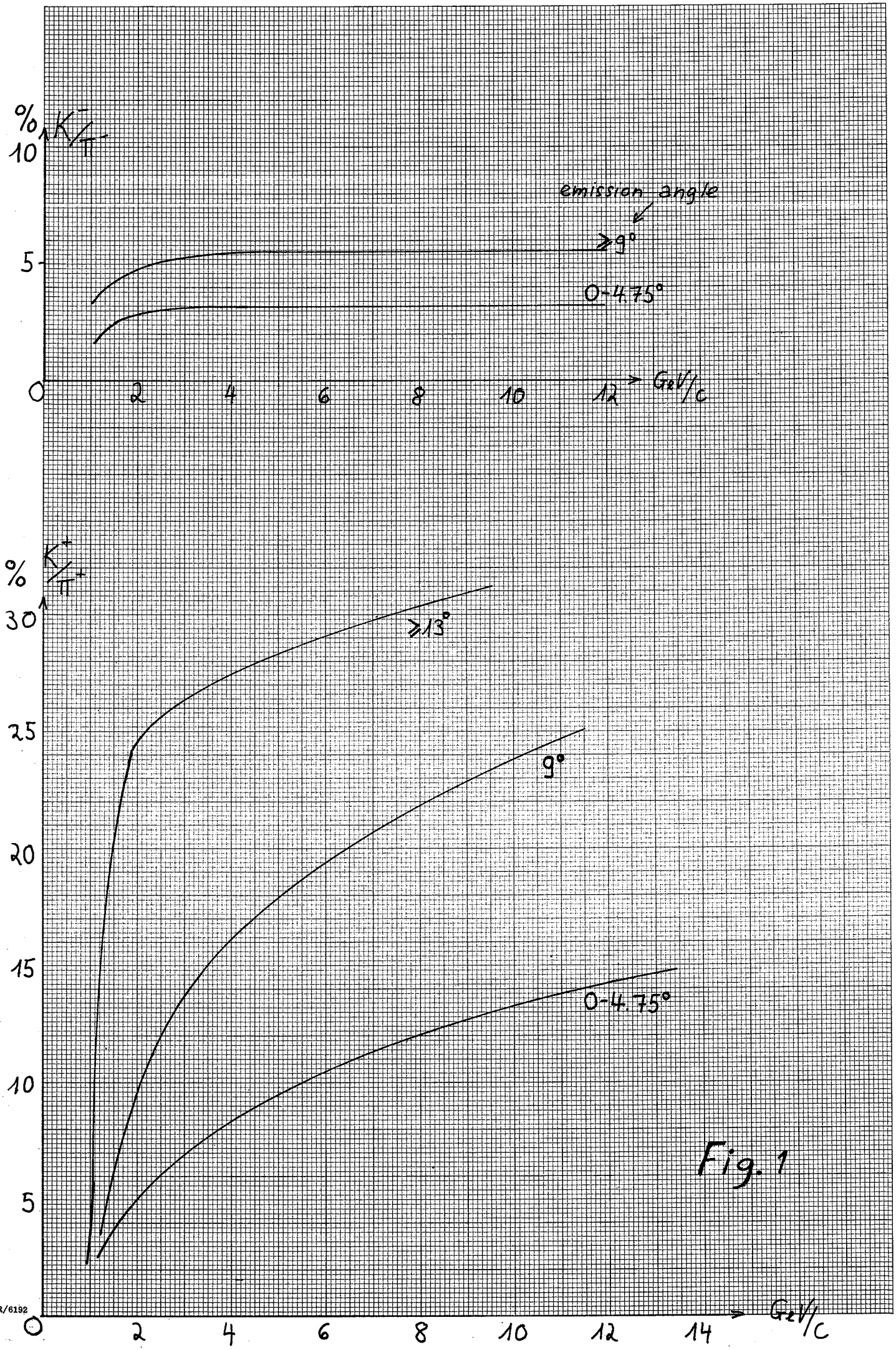
%
K^-/π^-
10
5
0
emission angle
$\geq 9°$
0-4.75°
2
4
6
8
10
12
GeV/c
%
K^+/π^+
30
25
20
15
10
5
0
$\geq 13°$
9°
0-4.75°
2
4
6
8
10
12
14
GeV/c

Fig. 1

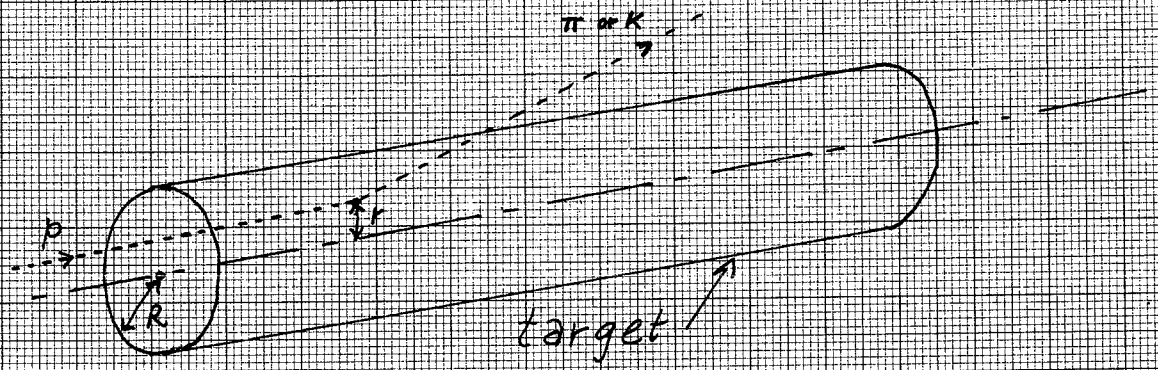
π or K
p
r
R
target

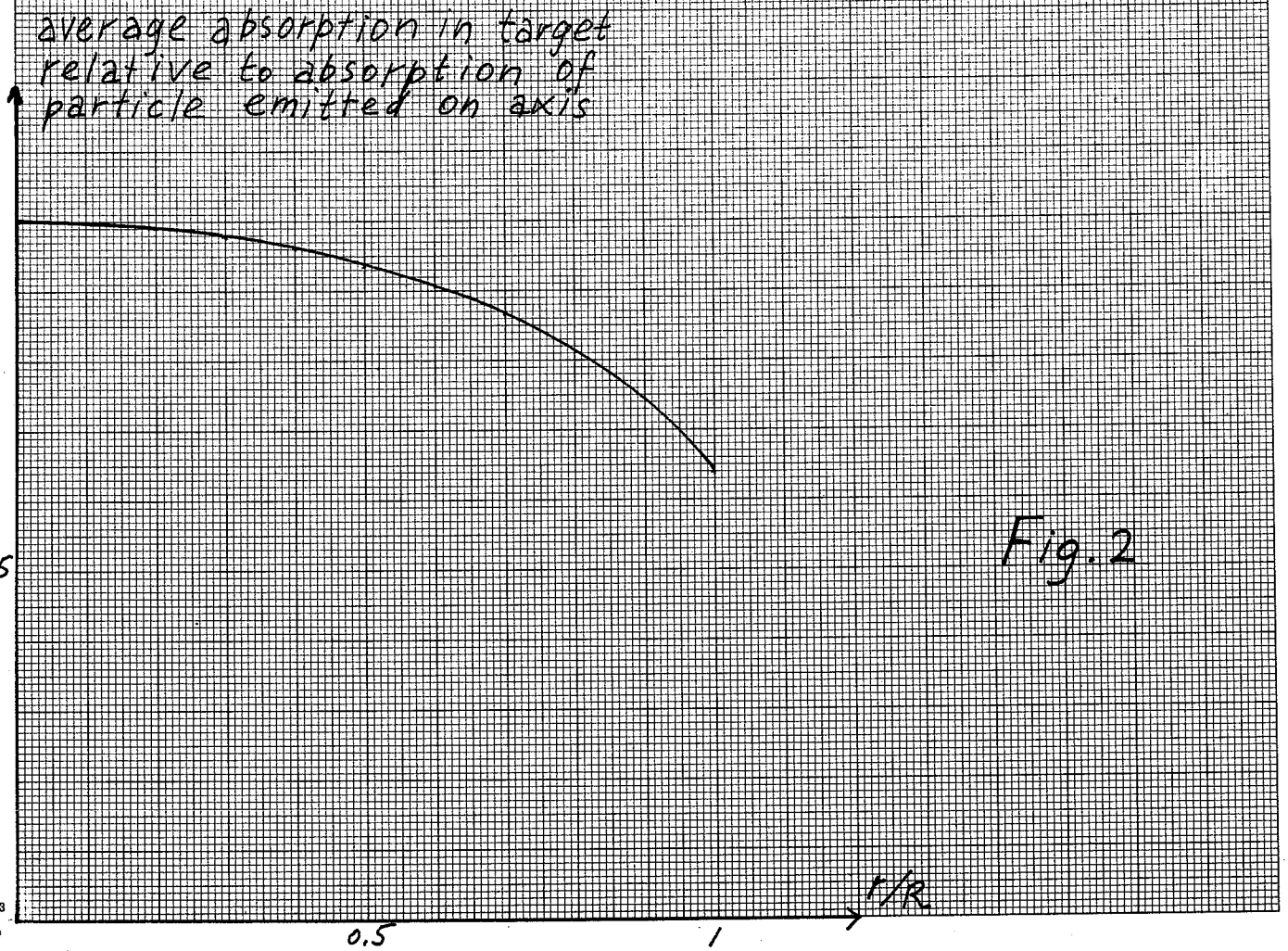
average absorption in target relative to absorption of particle emitted on axis
1
0.5
0
0.5
1
r/R

Fig. 2

SIS/R/6194

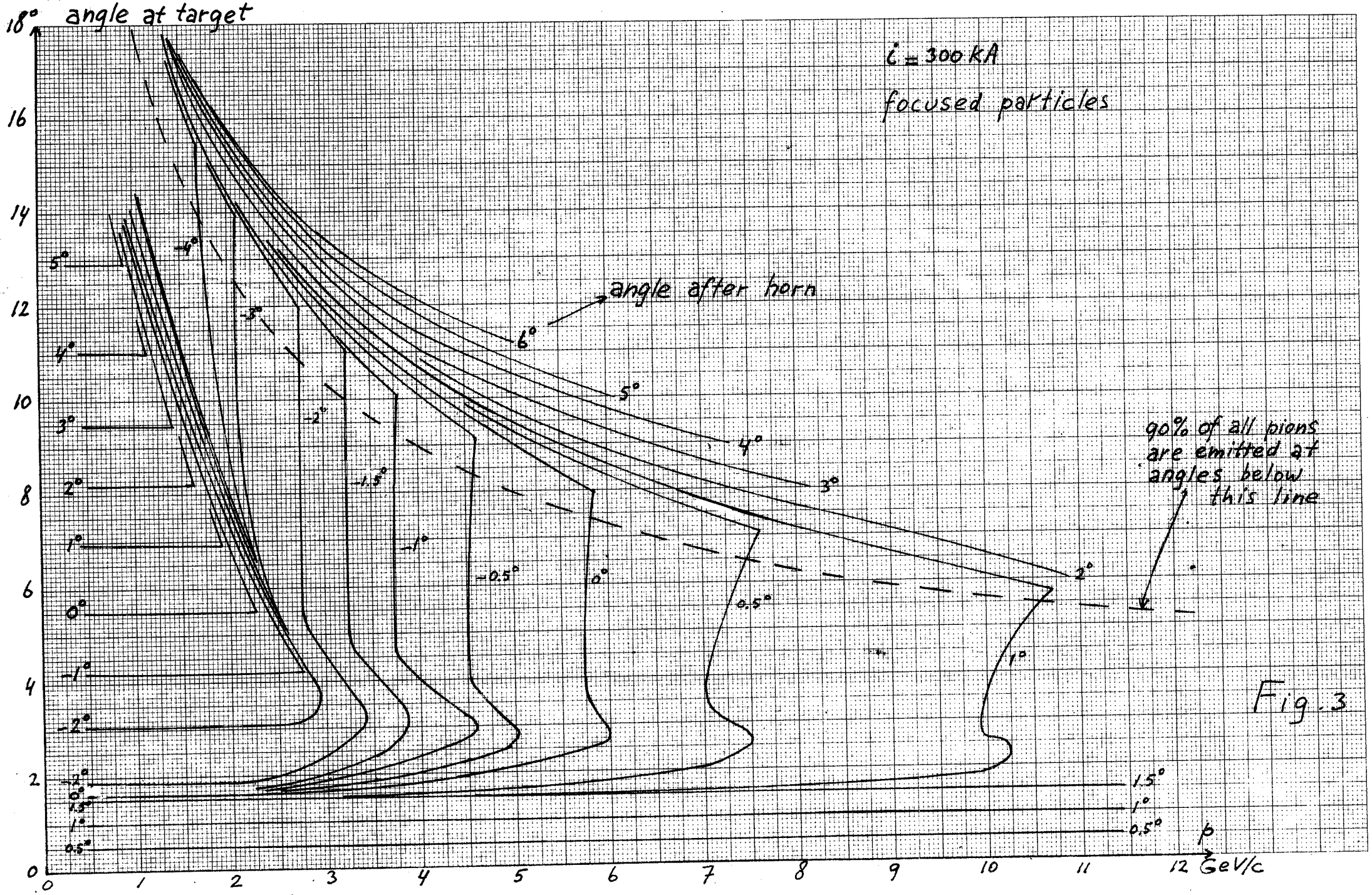

Fig. 3

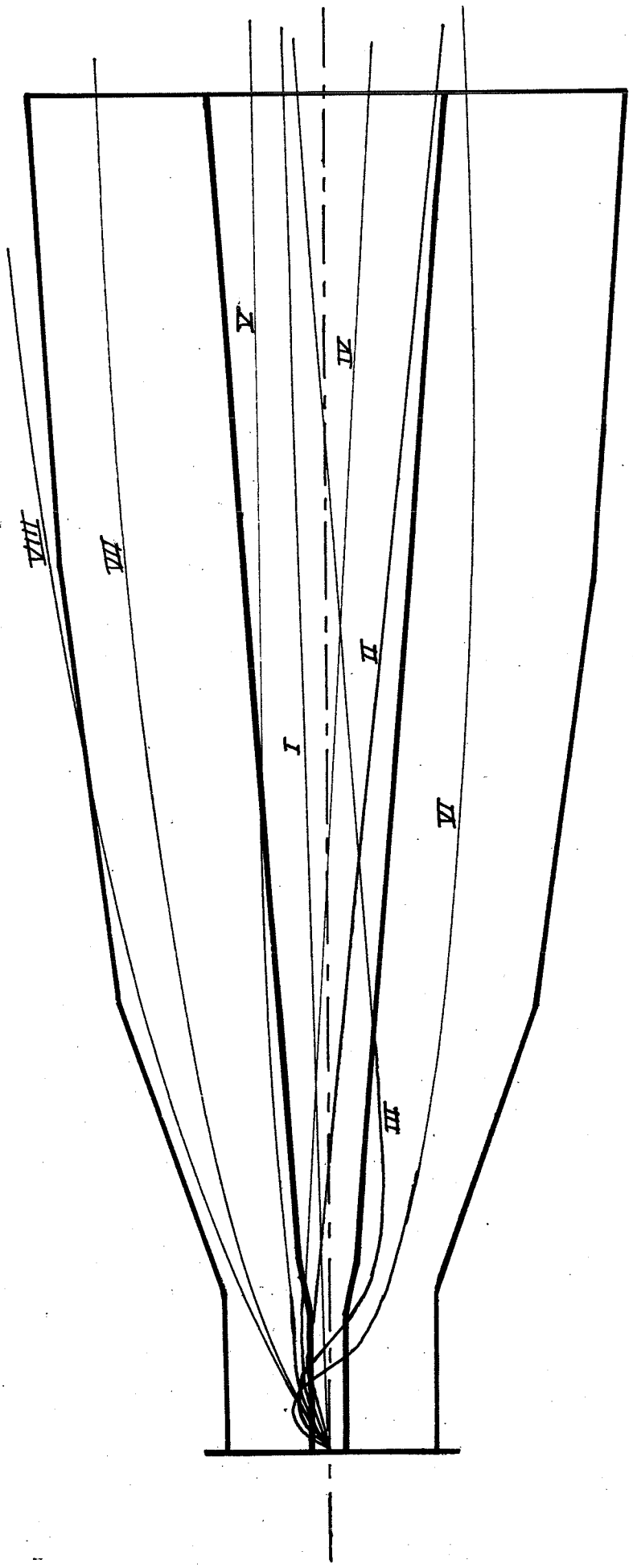

Fig. 4 (not drawn to scale)

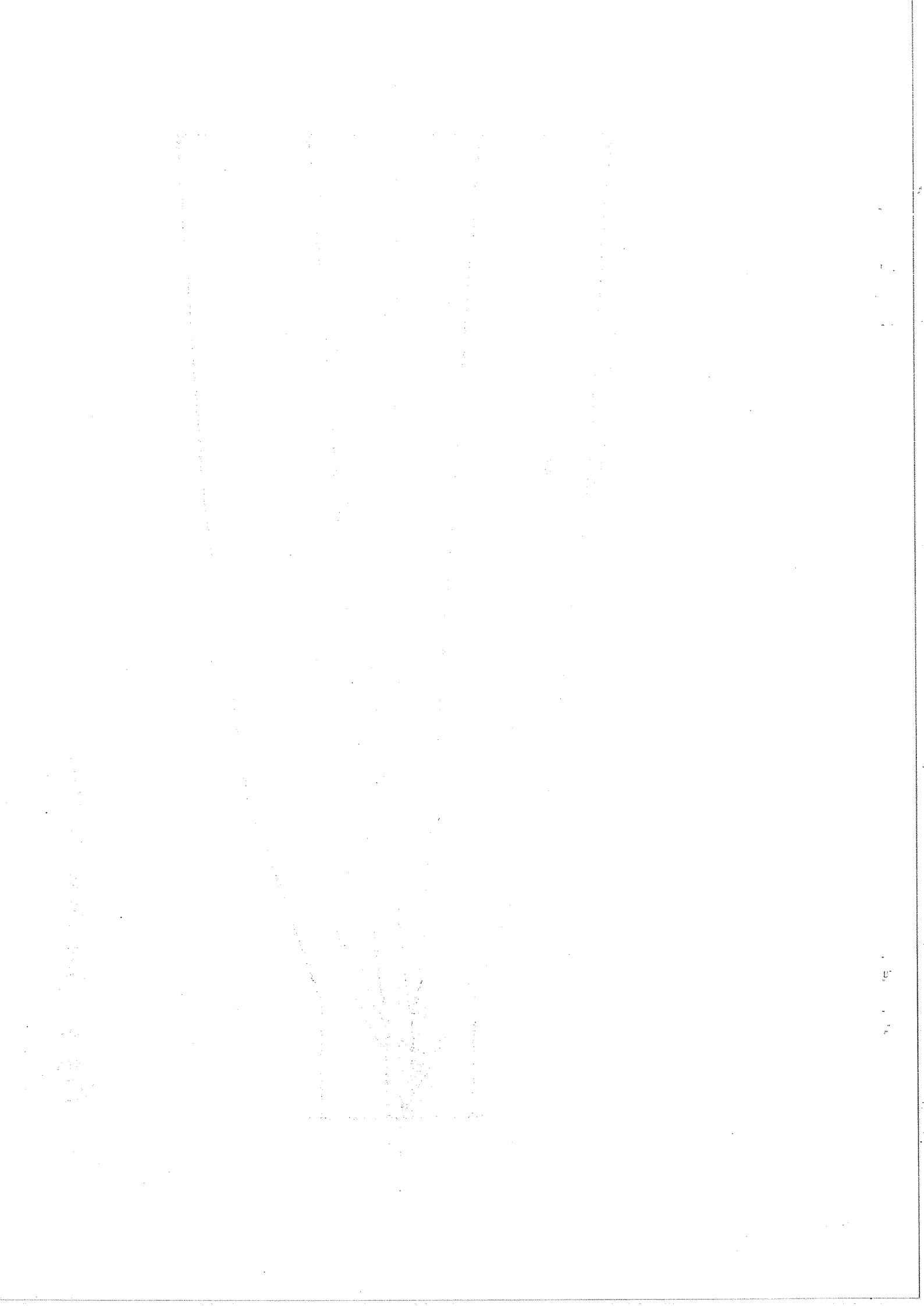

SES/R/6196

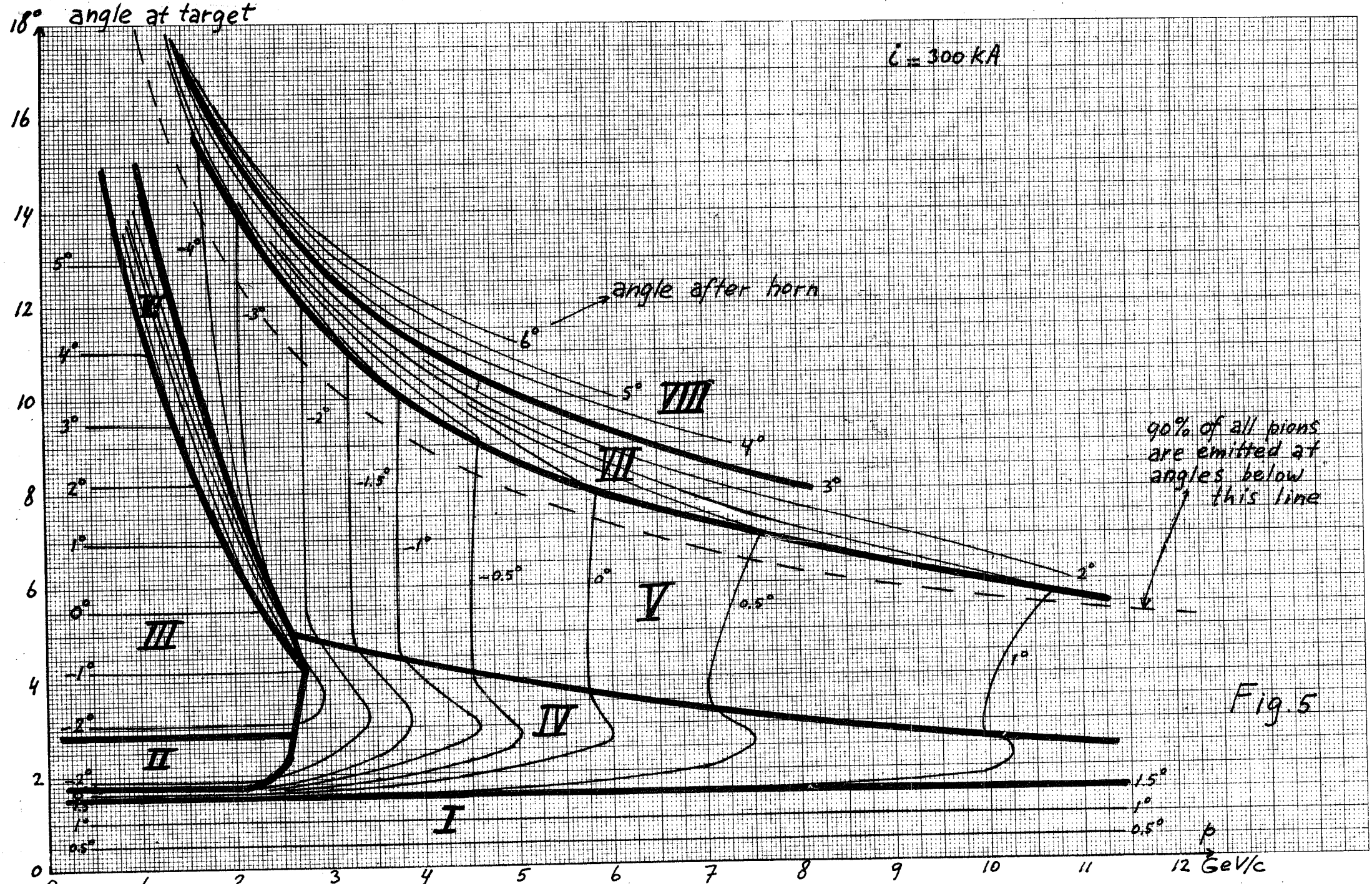

Fig. 5

SIS/R/6197

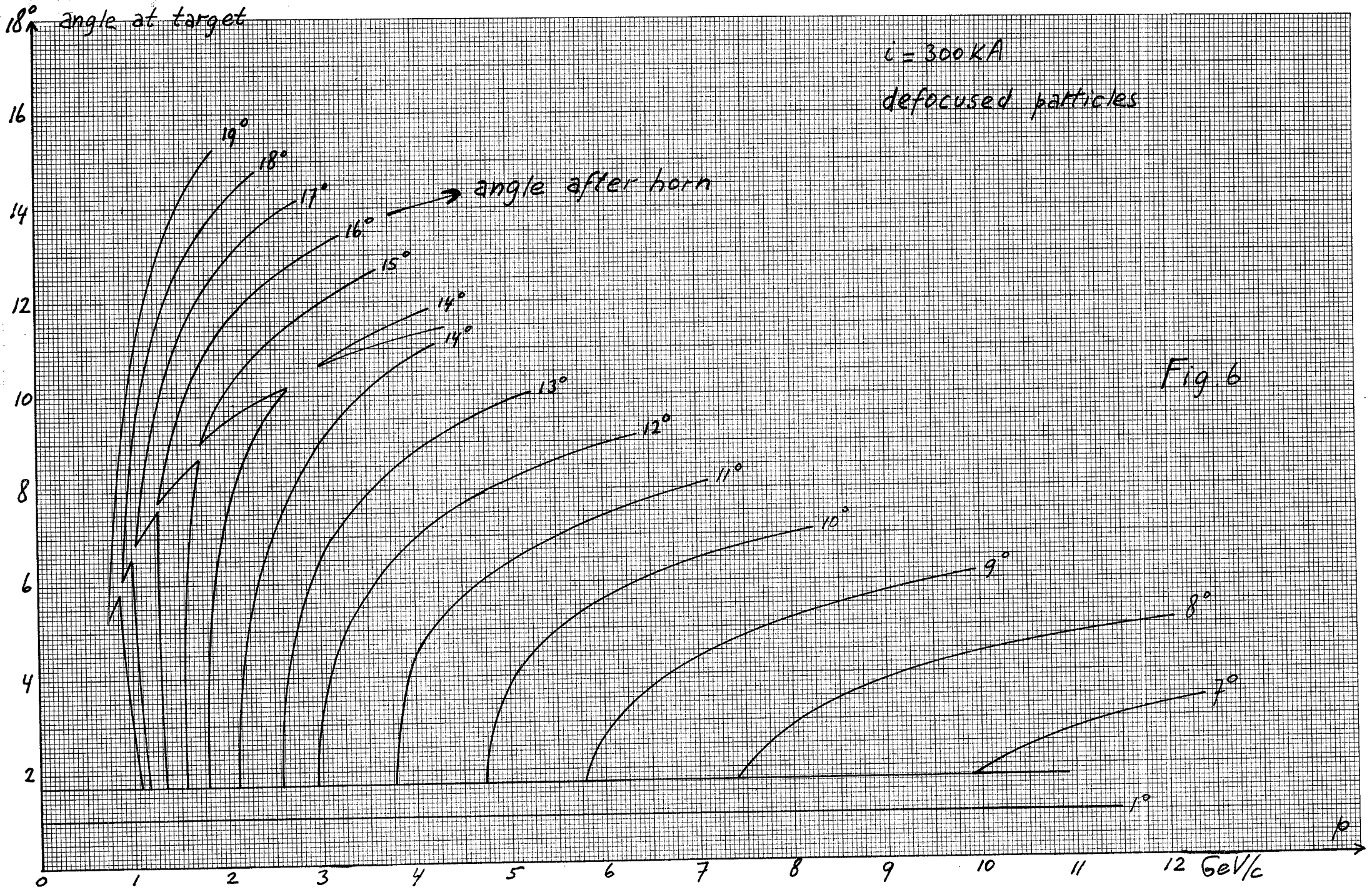

Fig 6

Fig. 7

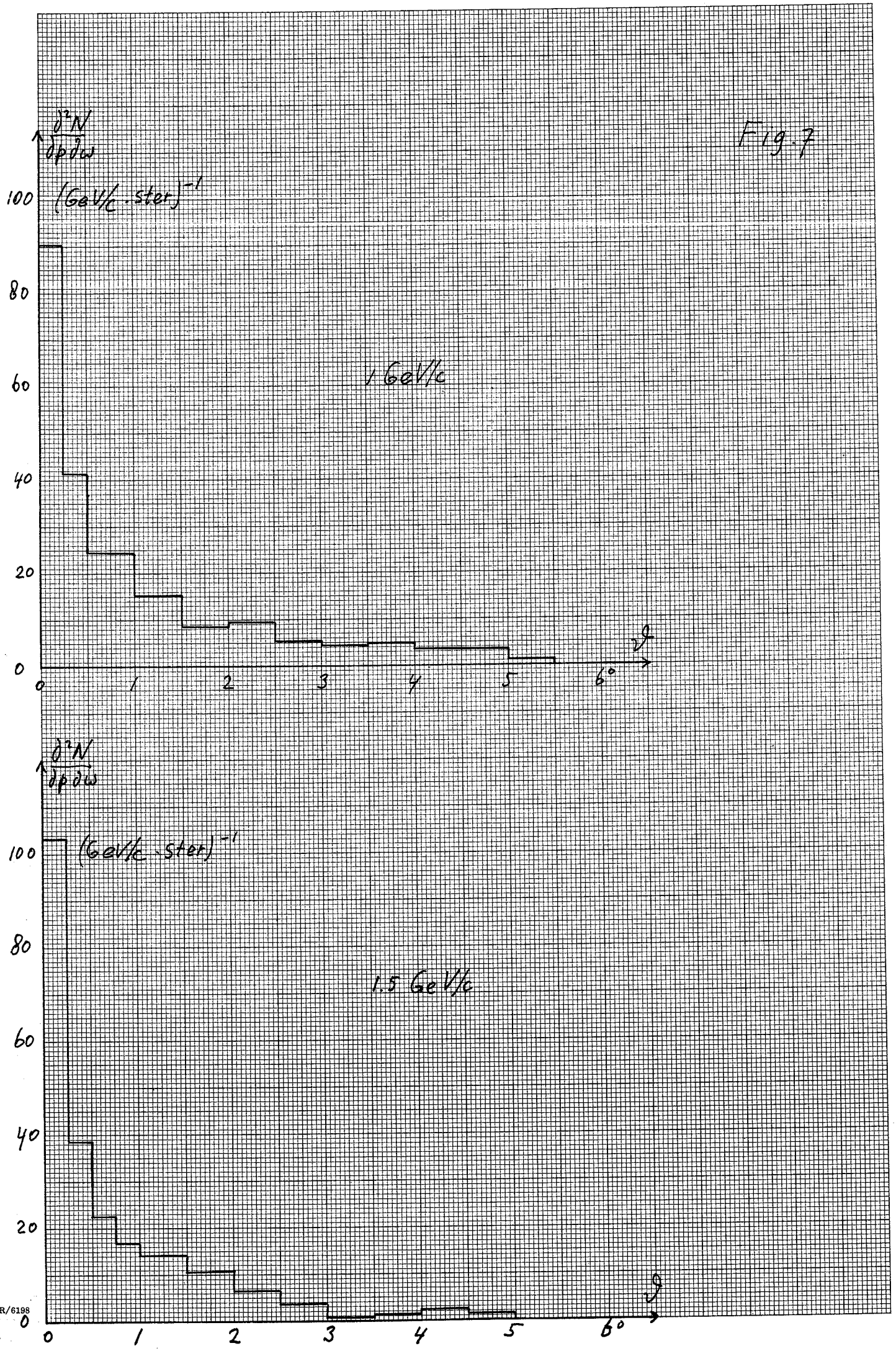
$\frac{\partial^2 N}{\partial p \partial \omega}$
(GeV/c . ster)$^{-1}$
100
80
60
40
20
0
1 GeV/c
0
1
2
3
4
5
6°
ϑ
$\frac{\partial^2 N}{\partial p \partial \omega}$
(GeV/c . ster)$^{-1}$
100
80
60
40
20
0
1.5 GeV/c
0
1
2
3
4
5
6°
ϑ

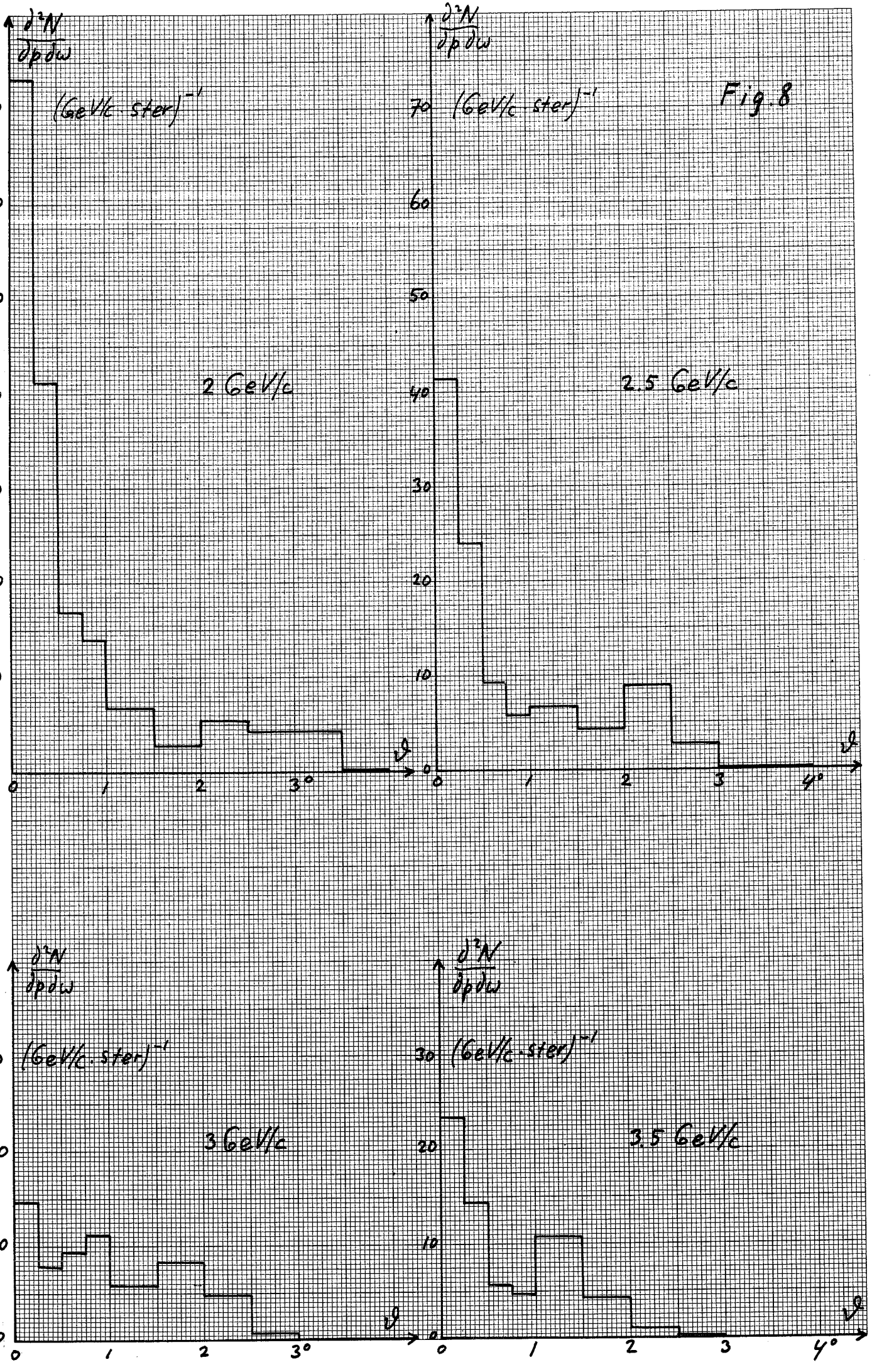

Fig. 8

SIS/R/6199

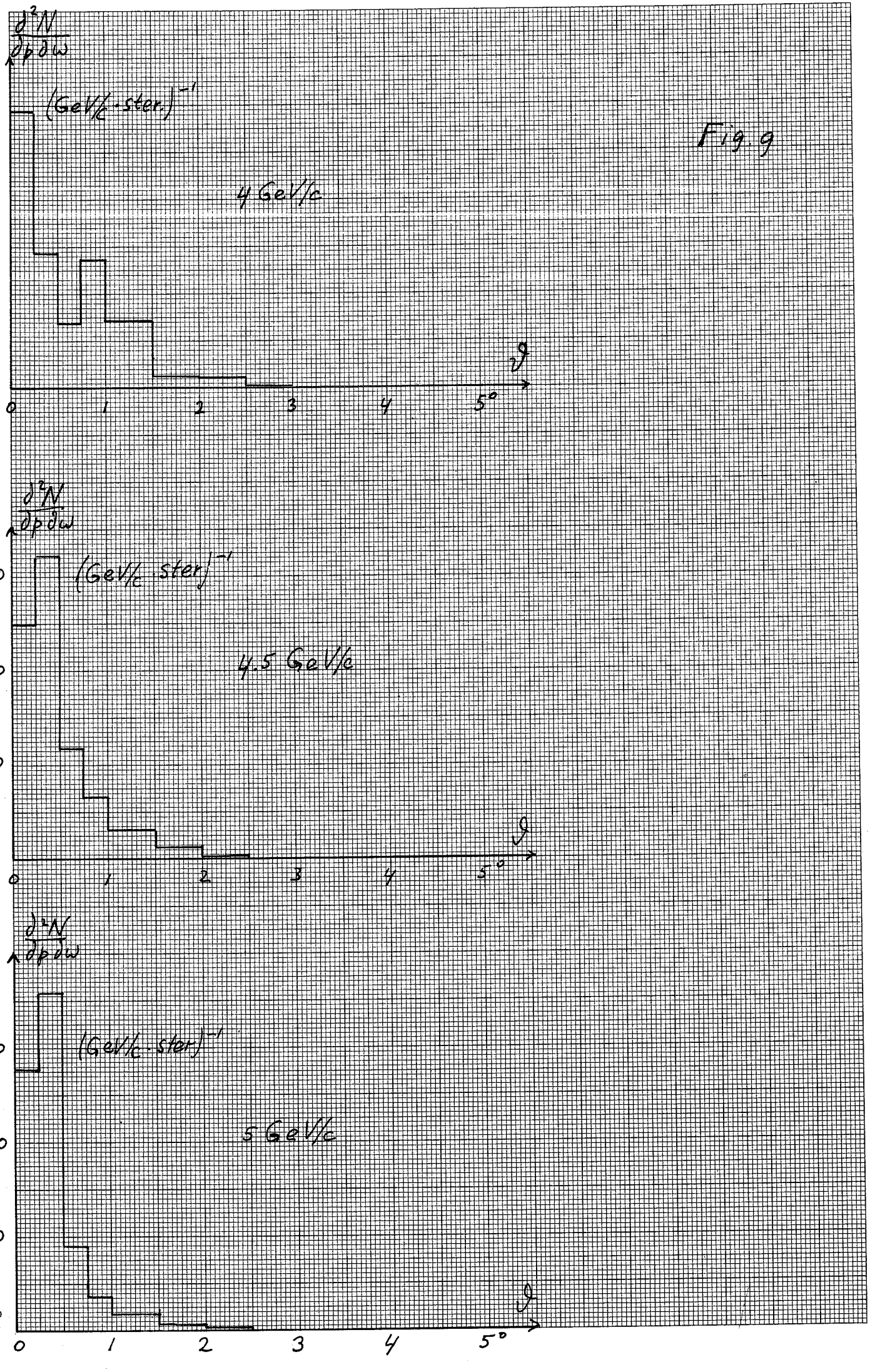
$\frac{d^2N}{dp\,d\omega}$
(GeV/c · ster)$^{-1}$
30
20
10
0
4 GeV/c
ϑ
0
1
2
3
4
5°
$\frac{d^2N}{dp\,d\omega}$
(GeV/c · ster)$^{-1}$
30
20
10
0
4.5 GeV/c
ϑ
0
1
2
3
4
5°
$\frac{d^2N}{dp\,d\omega}$
(GeV/c · ster)$^{-1}$
30
20
10
0
5 GeV/c
ϑ
0
1
2
3
4
5°

Fig 9

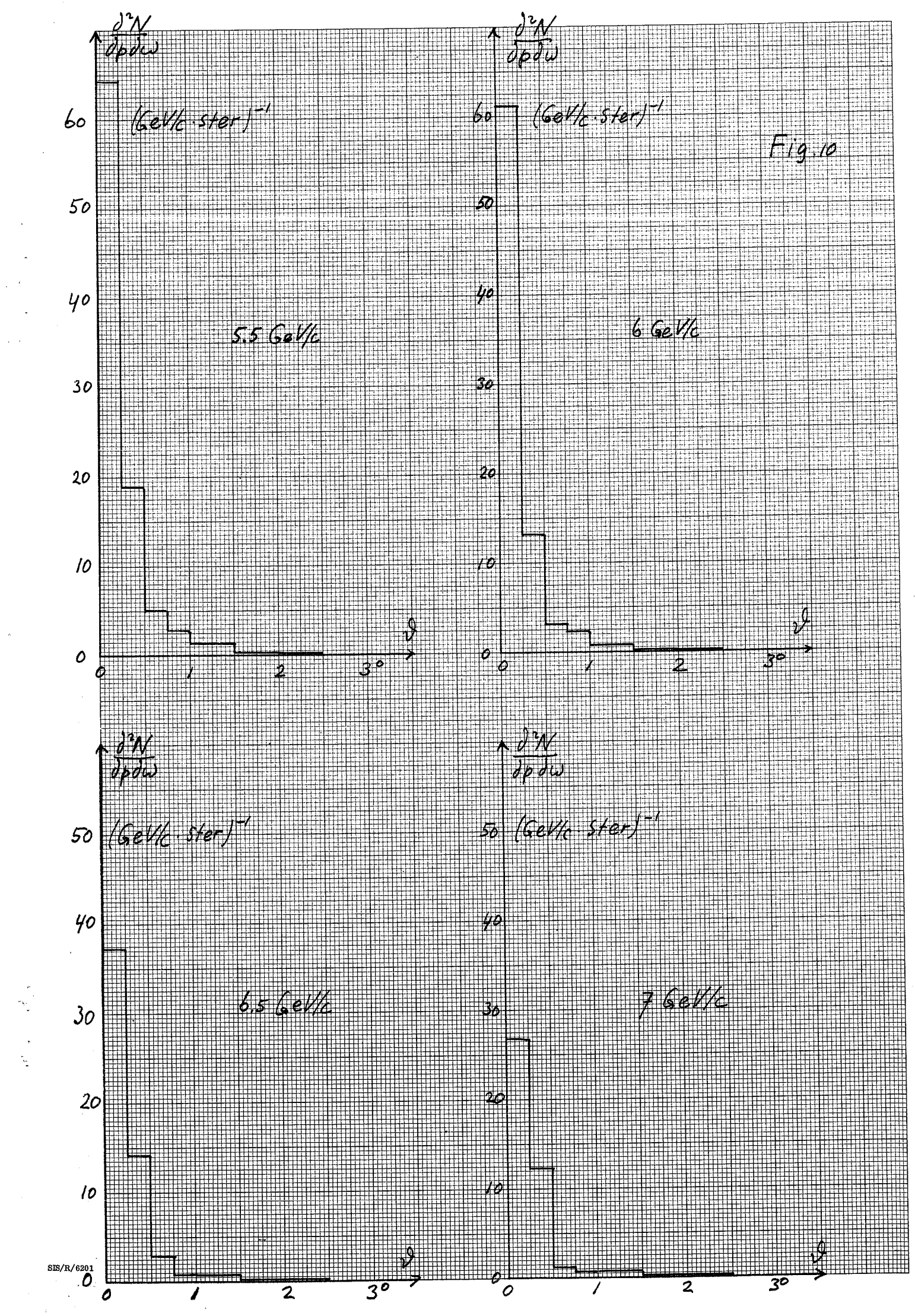
$\frac{d^2N}{dp\,d\omega}$
(GeV/c · ster)$^{-1}$
5.5 GeV/c
6 GeV/c
6.5 GeV/c
7 GeV/c
ϑ
0
1
2
3°
10
20
30
40
50
60

Fig. 10

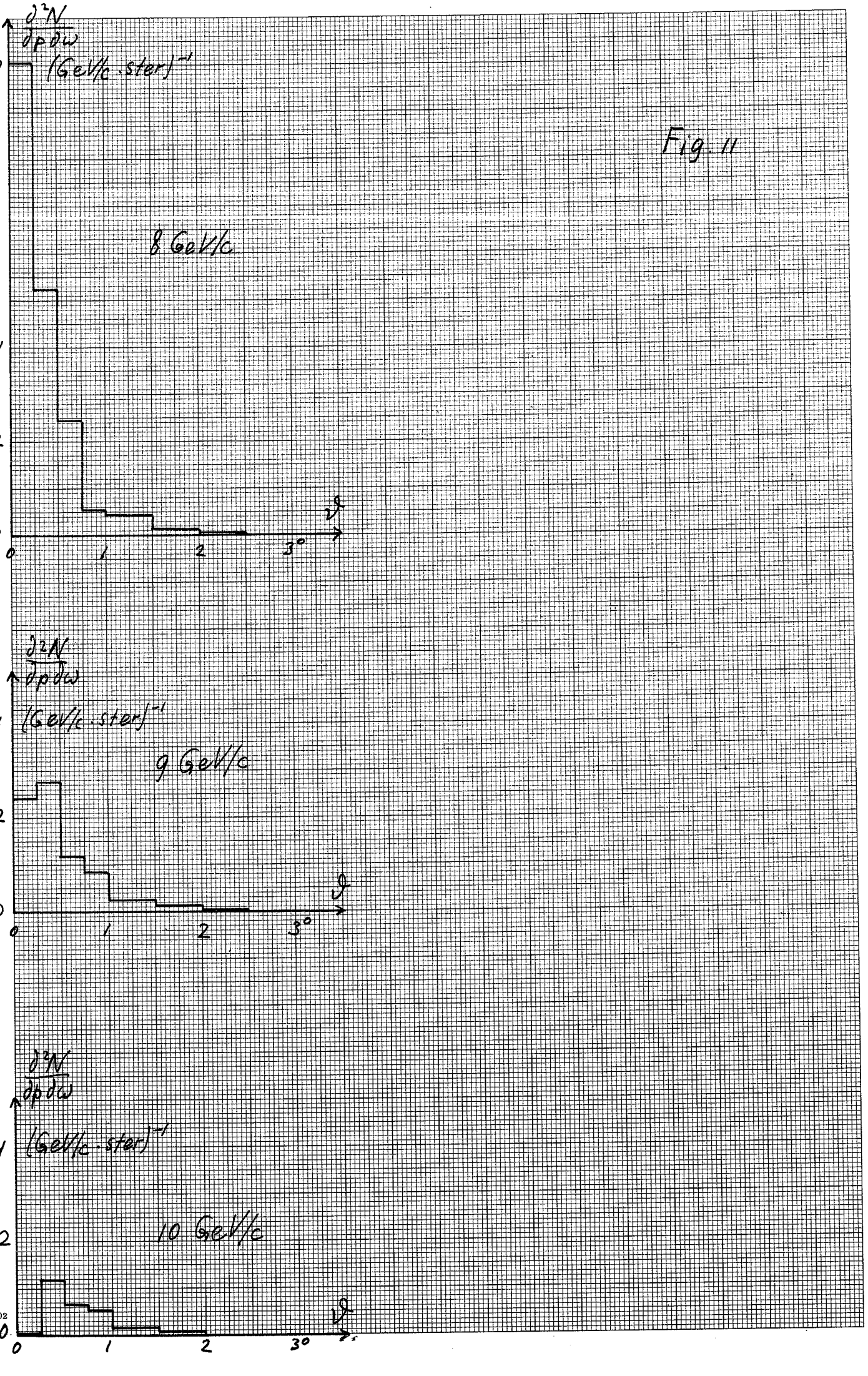
$\frac{\partial^2 N}{\partial p\, \partial \omega}$
(Gev/c . ster)$^{-1}$
10
8
6
4
2
0
8 GeV/c
ϑ
0
1
2
3°
$\frac{\partial^2 N}{\partial p\, \partial \omega}$
(Gev/c . ster)$^{-1}$
4
2
0
9 GeV/c
ϑ
0
1
2
3°
$\frac{\partial^2 N}{\partial p\, \partial \omega}$
(Gev/c . ster)$^{-1}$
4
2
0
10 GeV/c
ϑ
0
1
2
3°

Fig. 11

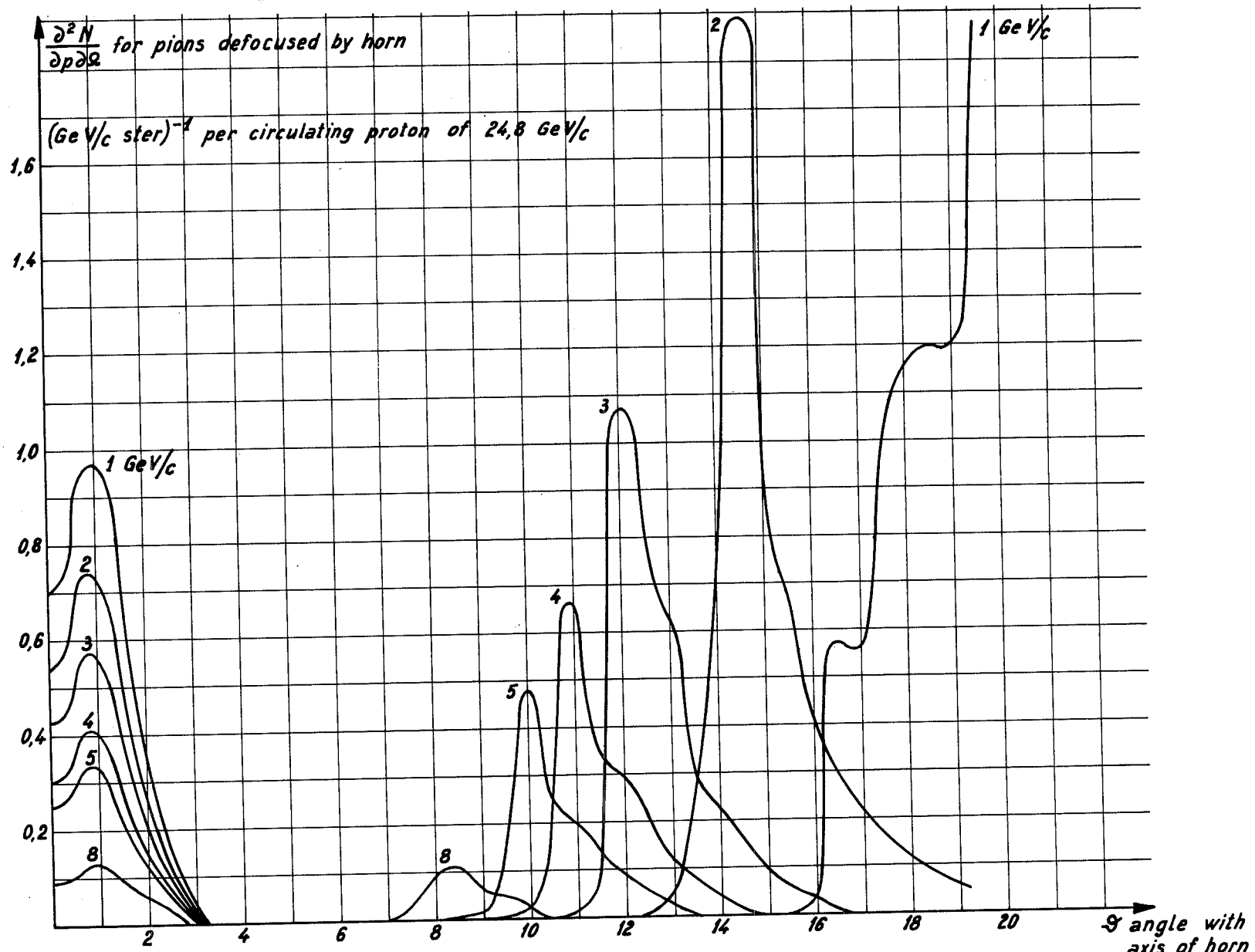
$\frac{\partial^2 N}{\partial p \partial \Omega}$ for pions defocused by horn
(GeV/c ster)$^{-1}$ per circulating proton of 24,8 GeV/c
1,6
1,4
1,2
1,0
0,8
0,6
0,4
0,2
1 GeV/c
2
3
4
5
8
2
4
6
8
10
12
14
16
18
20
ϑ angle with axis of horn

Fig.12

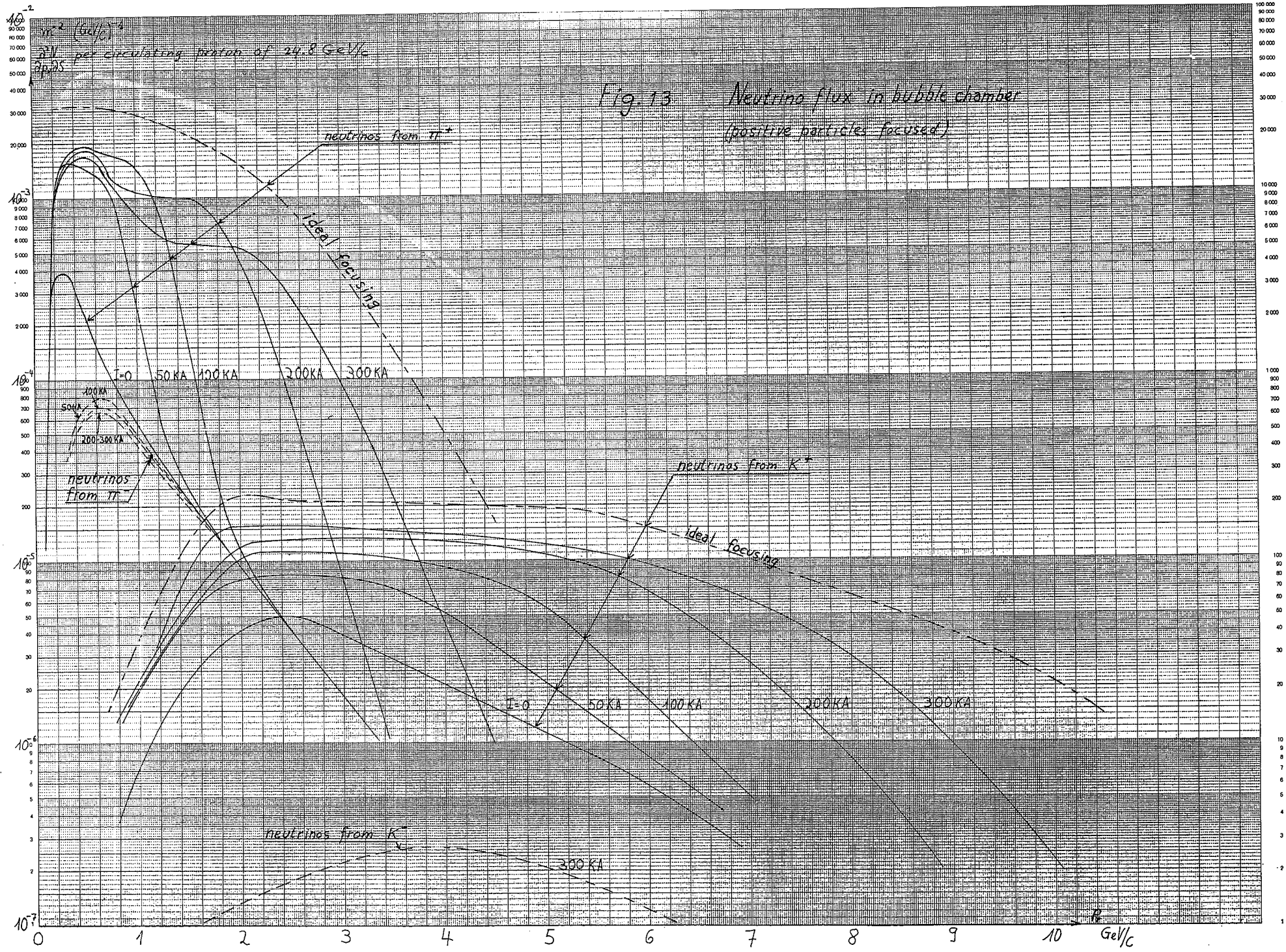

Fig. 13 Neutrino flux in bubble chamber (positive particles focused)

SIS/R/6204

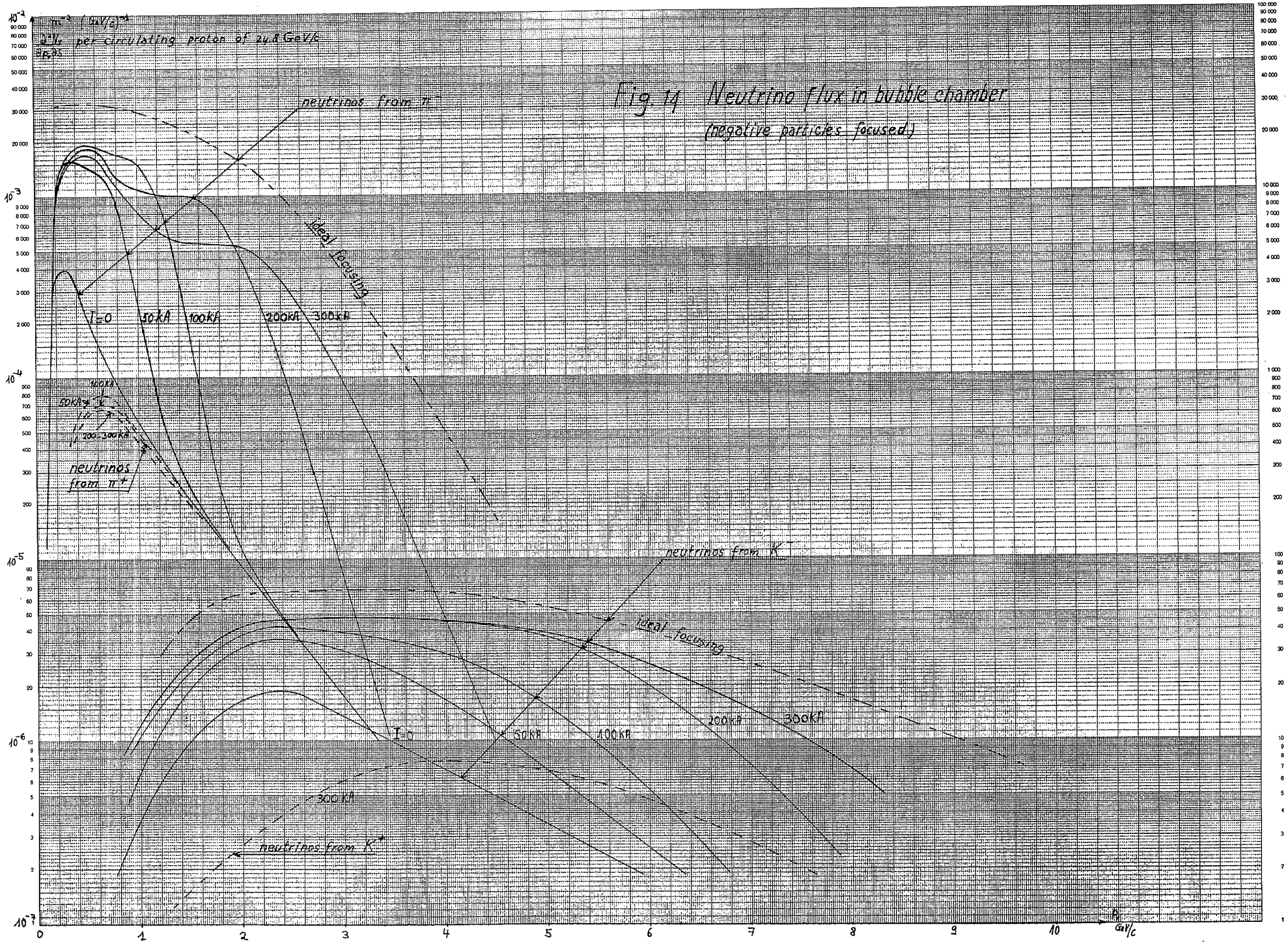

Fig. 14 Neutrino flux in bubble chamber
(negative particles focused)

SIS/R/6205

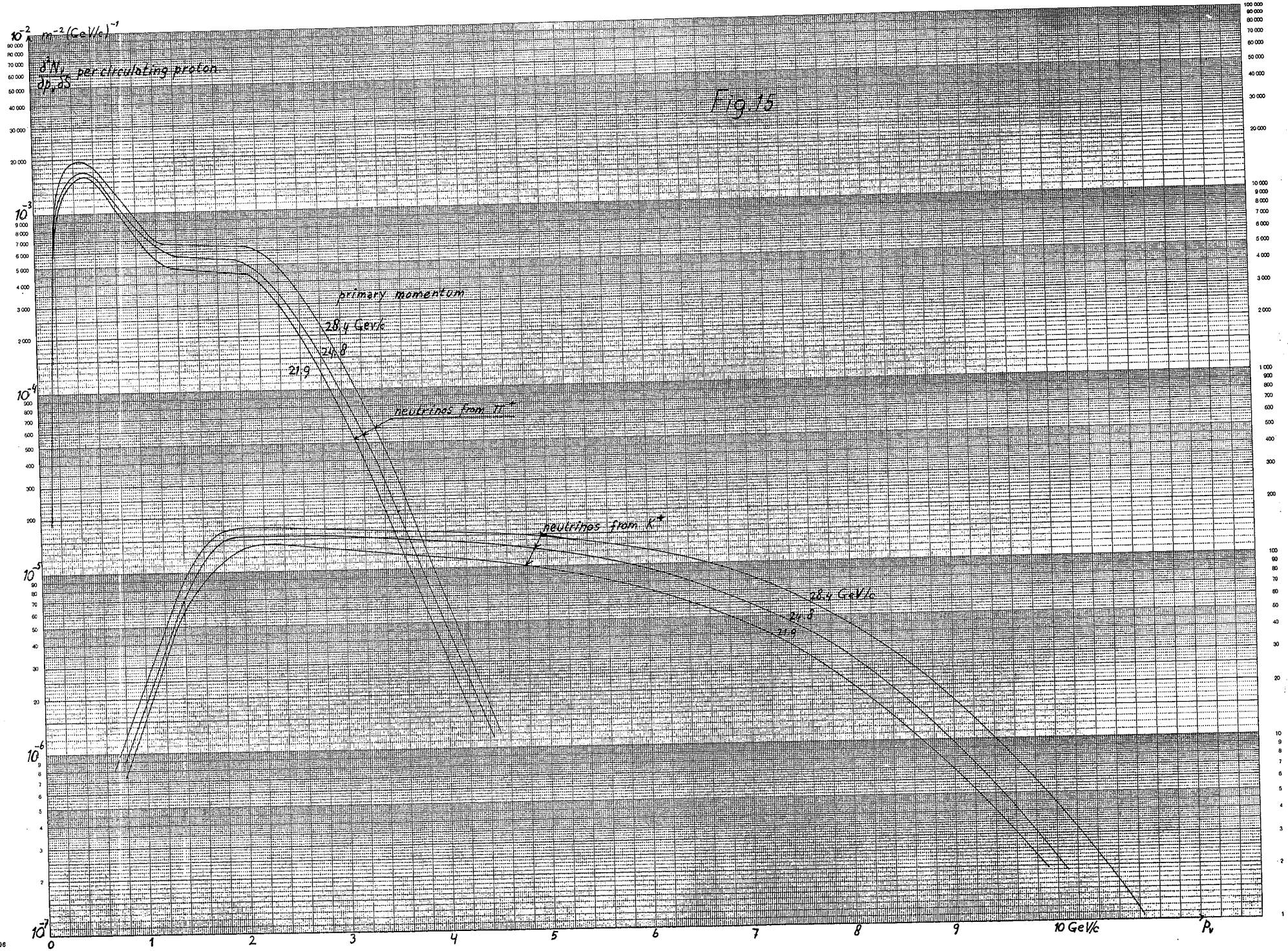
10^{-2} $m^{-2}(GeV/c)^{-1}$
$\frac{\partial^2 N_\nu}{\partial p_\nu \partial \Omega}$ per circulating proton
Fig. 15
primary momentum
28.4 Gev/c
24.8
21.9
neutrinos from π^+
neutrinos from K^+
28.4 GeV/c
24.8
21.9
10^{-3}
10^{-4}
10^{-5}
10^{-6}
10^{-7}
0
1
2
3
4
5
6
7
8
9
10 GeV/c
P_ν

SIS/R/6206

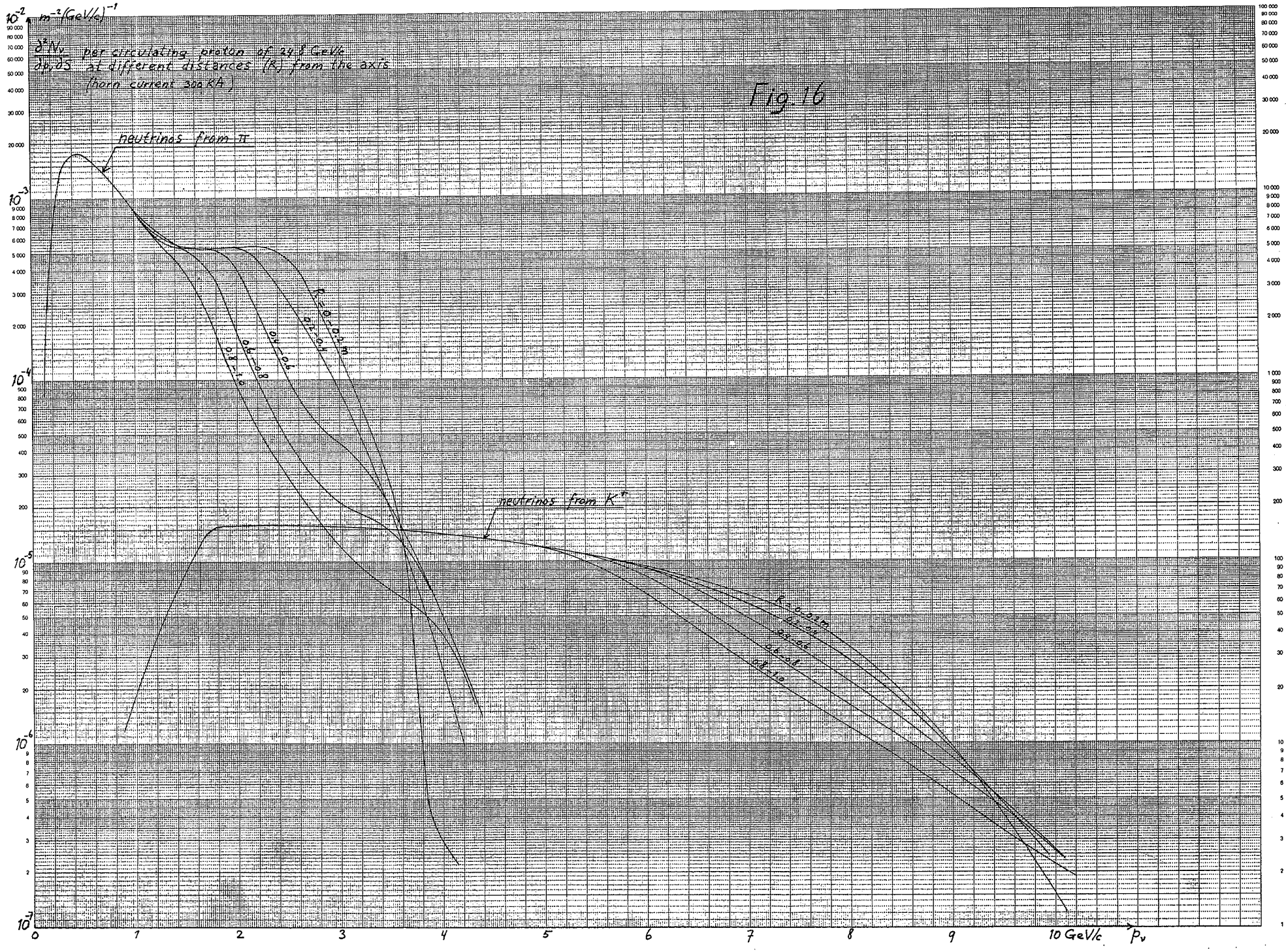
10^{-2} m^{-2}(GeV/c)$^{-1}$
$\frac{d^2N_\nu}{dp\,d\Omega}$ per circulating proton of 24.8 GeV/c
at different distances (R) from the axis
(horn current 300 KA)
Fig. 16
neutrinos from π
neutrinos from K
R = 0 – 0.2 m
0.2 – 0.4
0.4 – 0.6
0.6 – 0.8
0.8 – 1.0
1.0 – 1.2
10^{-3}
10^{-4}
10^{-5}
10^{-6}
10^{-7}
0
1
2
3
4
5
6
7
8
9
10 GeV/c
p_ν

SIS/R/6207

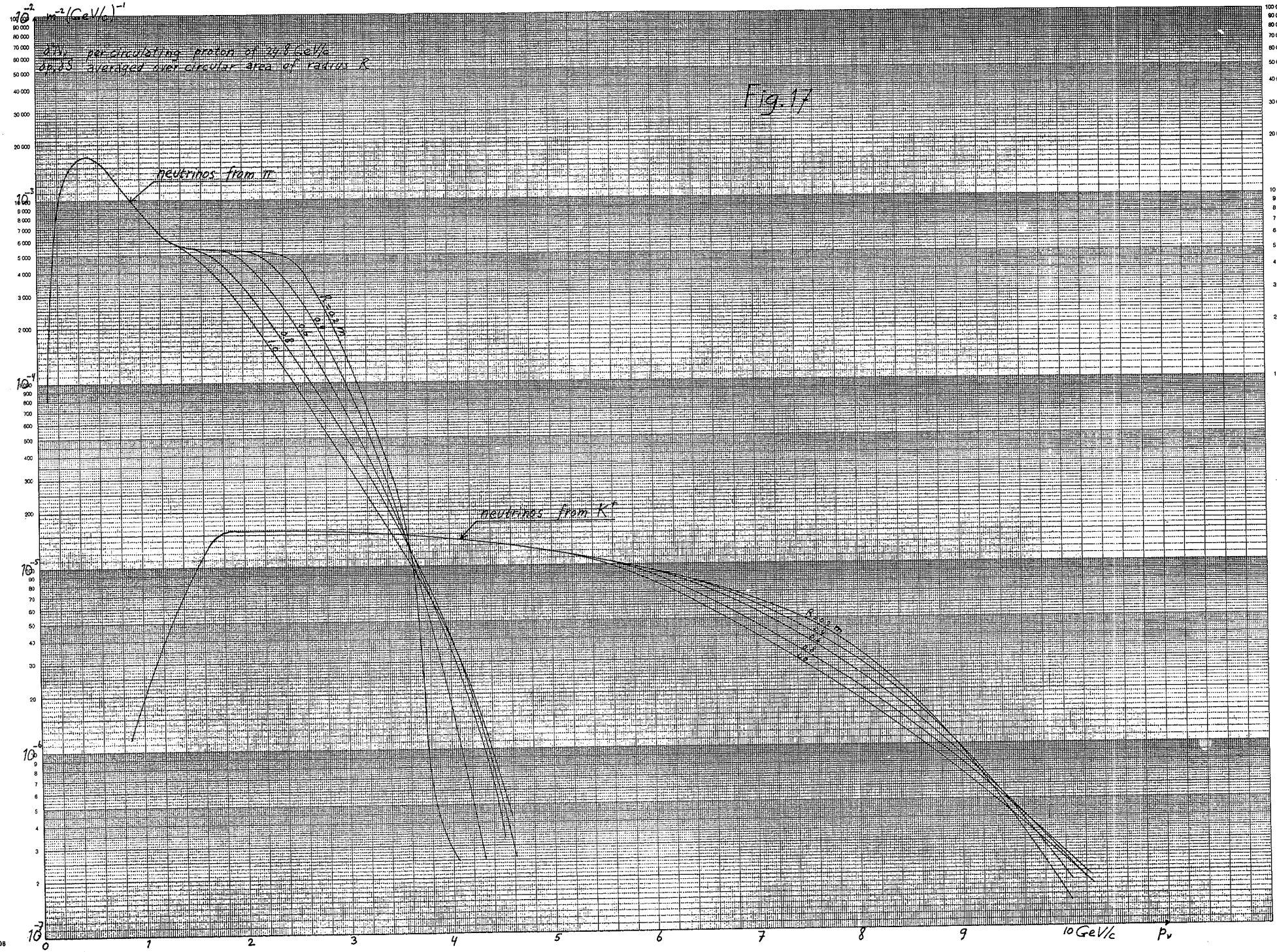

Fig. 17

SIS/R/6206

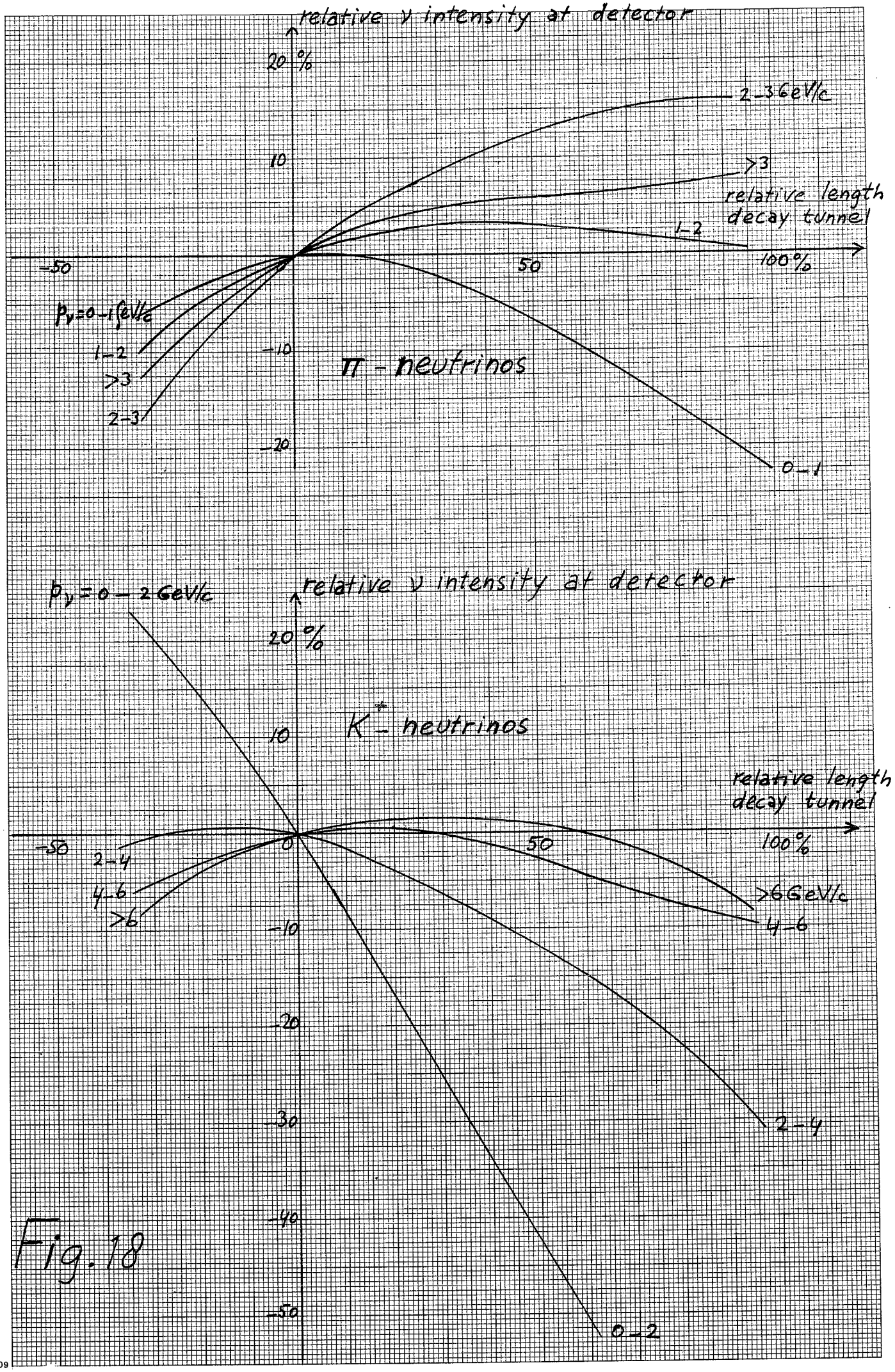

Fig. 18

SIS/R/6209

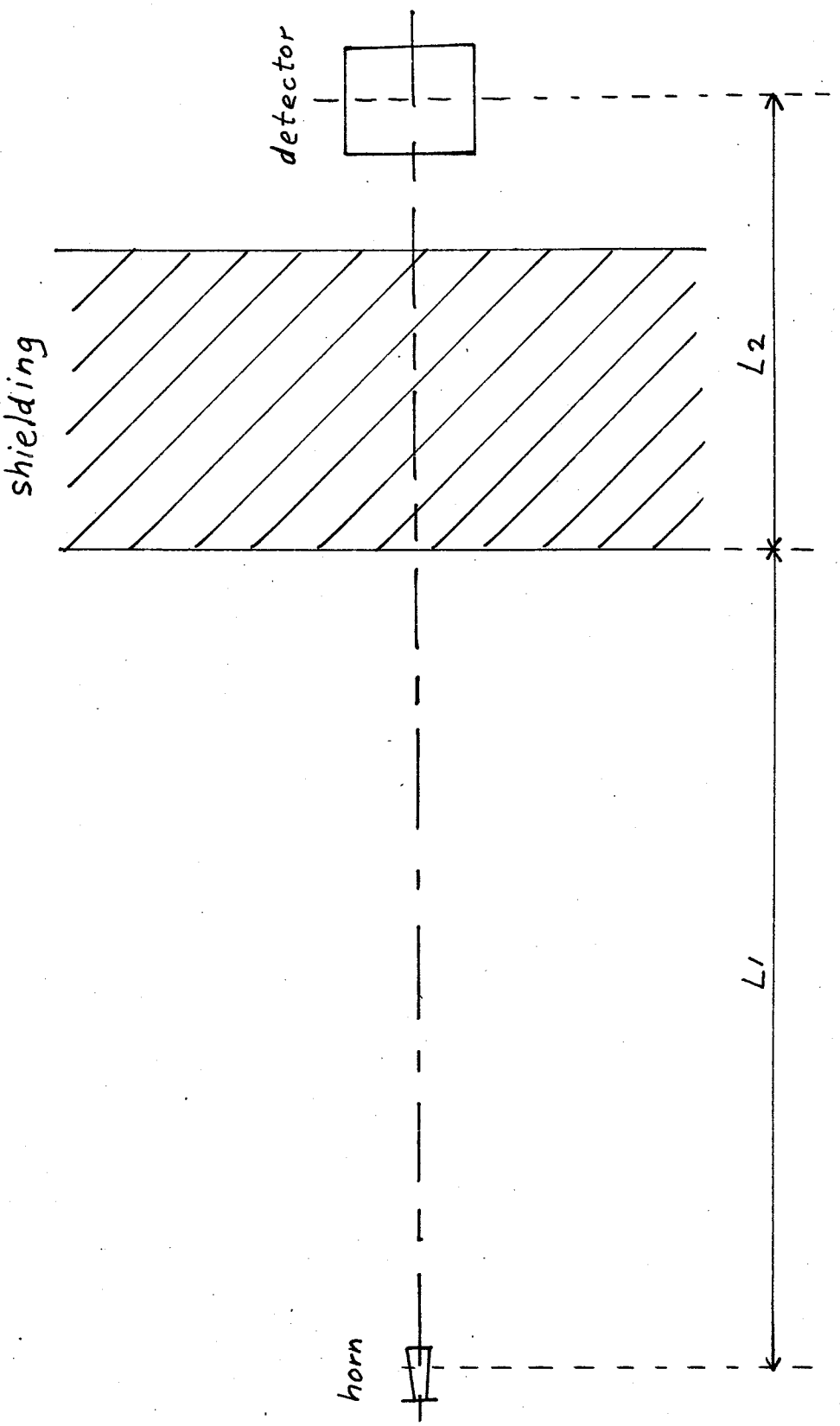

Fig. 19

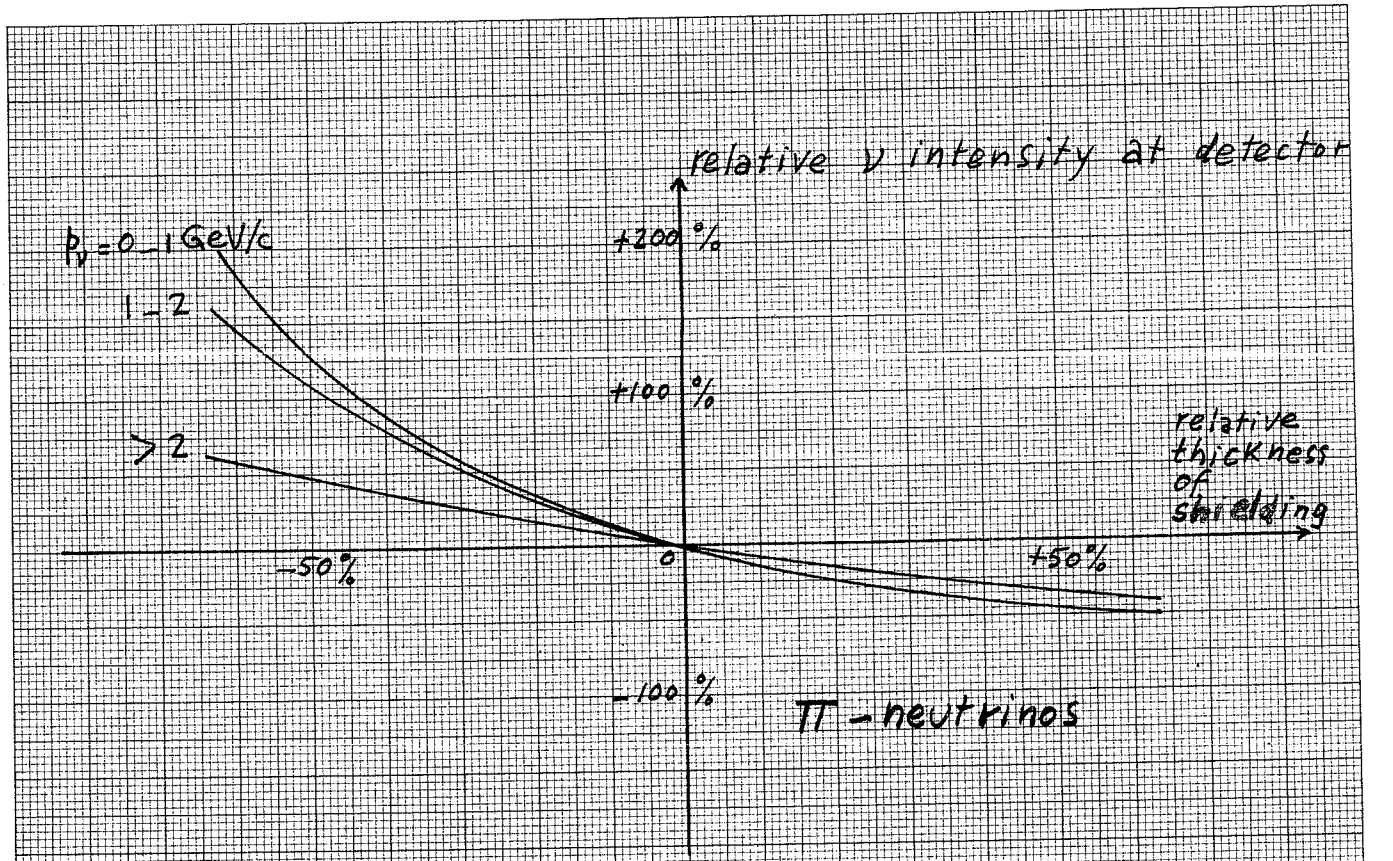
relative ν intensity at detector
p_ν = 0 - 1 GeV/c
1 - 2
> 2
+200 %
+100 %
-50 %
0
+50 %
-100 %
relative thickness of shielding
π - neutrinos

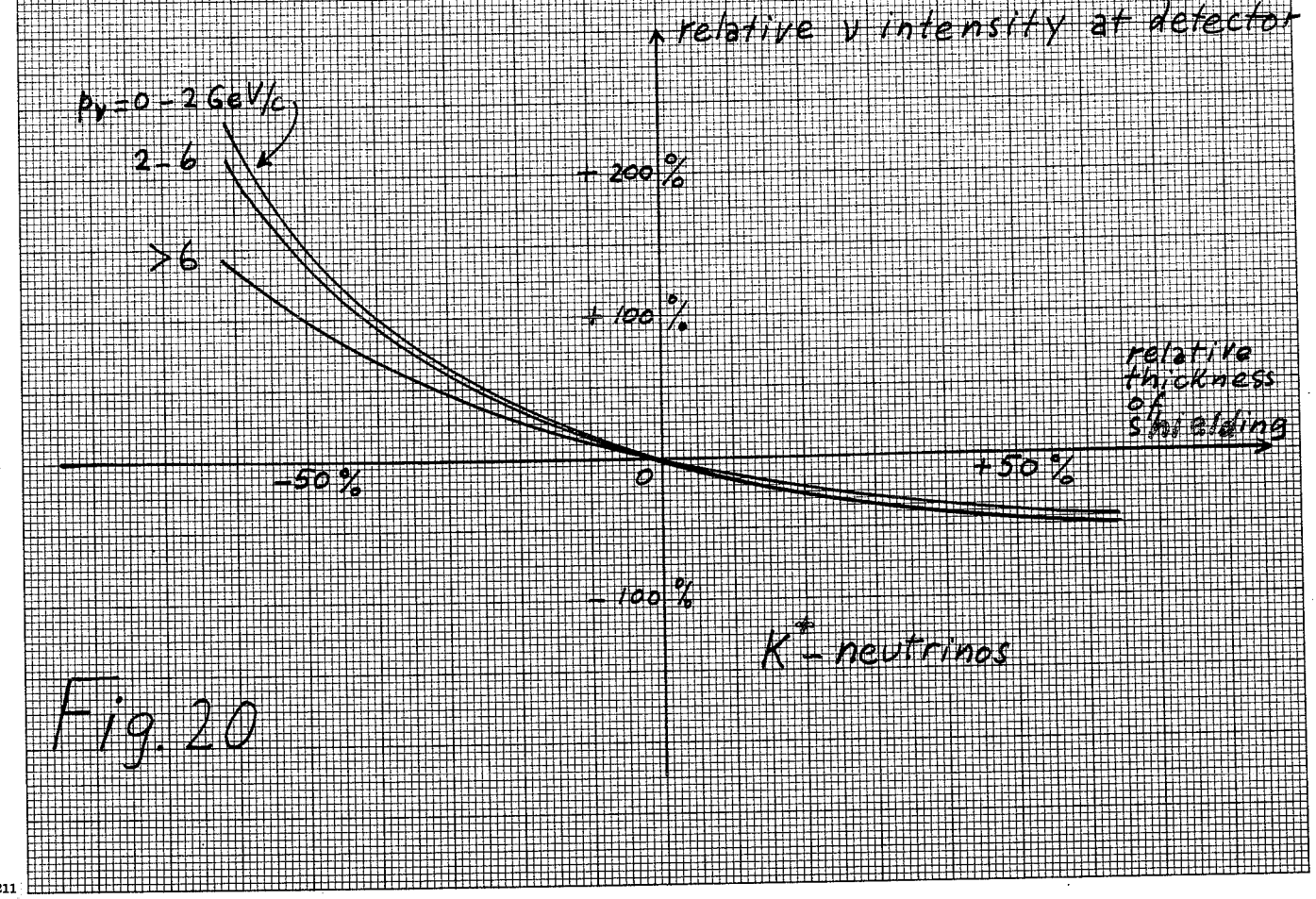
relative ν intensity at detector
p_ν = 0 - 2 GeV/c
2 - 6
> 6
+ 200 %
+ 100 %
-50 %
0
+50 %
- 100 %
relative thickness of shielding
K* - neutrinos

Fig. 20

SIS/PA/6212

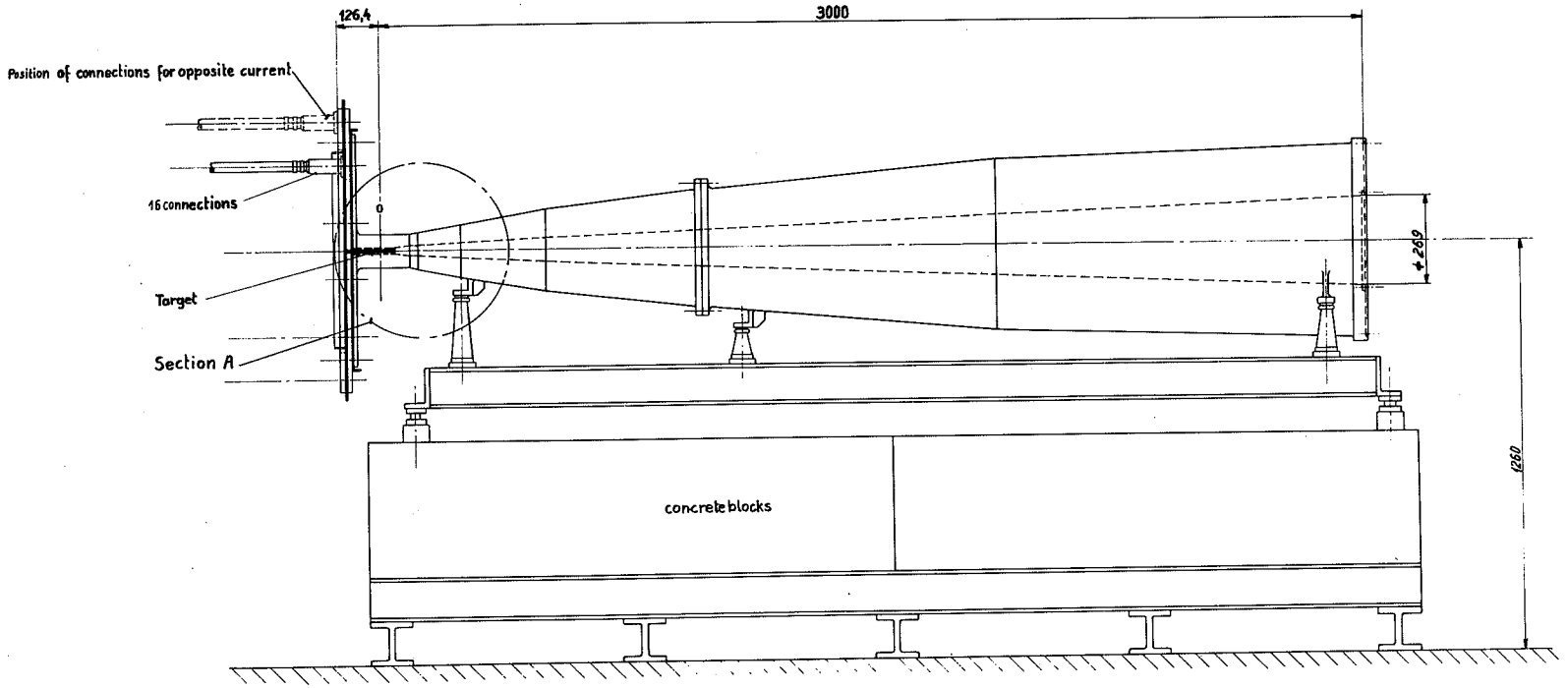

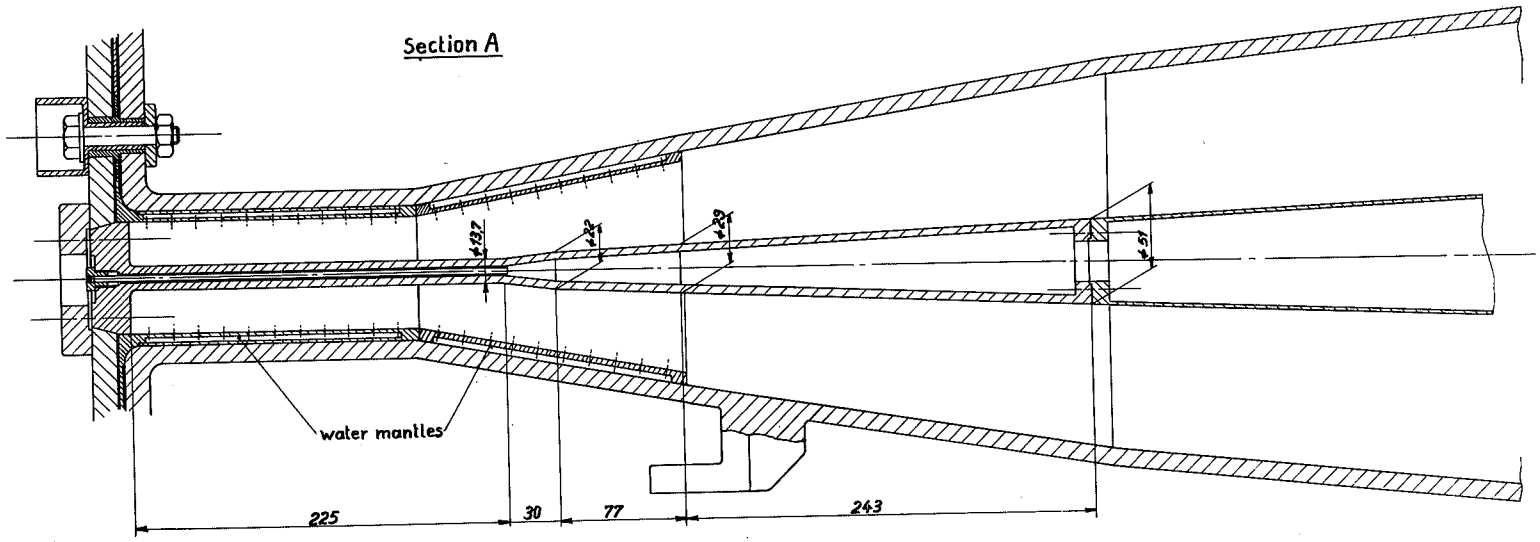

Fig. 21

Magnetic horn

P. 47- 106 - 2 A

9.5.63